Excited state absorption in chromium doped $Li_2B_4O_7$ glass

2001 J. Phys.: Condens. Matter 13 2701

(http://iopscience.iop.org/0953-8984/13/11/324)

INSTITUTE OF PHYSICS PUBLISHING JOURNAL OF PHYSICS: CONDENSED MATTER

J. Phys.: Condens. Matter **13** (2001) 2701–2716 www.iop.org/Journals/cm PII: S0953-8984(01)15469-X

Excited state absorption in chromium doped $Li_2B_4O_7$ glass

Cz Koepke[1], K Wisniewski[1], M Grinberg[2], A Majchrowski[3] and T P J Han[4]

[1] Institute of Physics, N Copernicus University, Grudziadzka 5/7, 87-100 Toruń, Poland
[2] Institute of Experimental Physics, University of Gdansk, Wita Stwosza 57, 80-952 Gdańsk, Poland
[3] Institute of Physics, Military University of Technology, Kaliskiego 2, 00-908 Warszawa, Poland
[4] Department of Physics and Applied Physics, Strathclyde University, Colville Building, Glasgow G1 1XN, UK

Received 13 July 2000, in final form 3 January 2001

Abstract

Excited state absorption (ESA) measurements of the Cr:$Li_2B_4O_7$ glass (Cr:LBO-glass) along with preliminary interpretation are presented. The presence of chromium in its tri- (d^3) and hexa- (d^0) valence states is observed. Both Cr^{3+} and Cr^{6+} ions appear to contribute in the de-excitation processes and can be attributed in the ESA spectra under excitation wavelengths at 308 nm, 488 nm, 515 nm and 610 nm. The ESA spectra detected with UV excitation have been interpreted in terms of transitions in the framework of the $Cr^{5+}O^-$ centre, which forms after charge-transfer-type absorption in the $[CrO_4]^{2-}$ group. Assumption of the double-electron state of the $3d^22p^4$ electronic configuration together with crystal-field-split states of the $3d^12p^5$ configuration allowed us to reproduce the obtained ESA spectra. The ESA spectra of the Cr^{3+} ions have different characteristics and are related to transitions to the conduction band.

1. Introduction

Lithium tetraborate ($Li_2B_4O_7$) is a well known material, which has found numerous optoelectronic applications [1–3] but so far it has not yet been used as a primary laser host or gain medium. This is because of the tight packing of the LBO single crystal lattice and the relatively large sizes of the dopant ions that are of interest, for example Cr^{3+} ions. However, in the glass matrix the situation is different. The glasses have more loose and relaxed structures and are more 'dopant friendly' allowing much higher concentration doping than in crystals. One of the most representative dopants is chromium, which had given rise to several successful lasers (e.g. [4–6]). The LBO-glass doped with chromium ions has been previously exploited by various authors [7–9] and considered as a possible laser medium; however direct measurements of the ESA, that are of the greatest and critical importance in this context, have not yet been done. In this paper, apart from basic spectroscopic characterization of the Cr:LBO-glass,

results of the ESA measurements along with preliminary interpretation are presented for the first time.

2. Material characterization and preparation

Single crystals of LBO are also known as substrates for surface acoustic wave (SAW) devices. The material has cuts with temperature stability of acoustic wave velocity and relatively high electromechanical coupling coefficient for SAW applications. Polycrystals of doped $Li_2B_4O_7$ also find applications in thermoluminescent personal dosimeters [10]. As mentioned above, owing to the small ionic radii of lithium and boron it is not possible to introduce dopants into $Li_2B_4O_7$ single crystals at high levels. The relatively high viscosity of molten lithium tetraborate, which is the case for most borates [11], posed a serious problem during single crystal growth of this material [12]. However, the fact that borates solidified readily in the glass phase, the large transparency range and the potential to incorporate high concentrations of dopant made it a good medium for investigations of optically active dopant ions.

Lithium tetraborate ($Li_2B_4O_7$) is congruently melting with a melting point at 917 °C. The synthesis of $Li_2B_4O_7$ glass was carried out from lithium carbonate, Li_2CO_3, and boric oxide, H_3BO_3 (Merck, extra pure), in platinum crucibles in air. After reaction of the starting materials at 950 °C the obtained compound was overheated to 1150 °C to remove traces of water and carbon dioxide, which were present in the melt. Because of B_2O_3 losses, due to evaporation, 1 mol% surplus of H_3BO_3 was added to the starting composition. Cr_2O_3 was dissolved into lithium tetraborate at the concentration of 0.15 mol%. After rapid cooling below 550 °C the melt formed a glass, which did not show any tendency to crystallize. The addition of chromium oxide caused green colouration of the glass. Prolonged heating of the obtained glass at temperatures higher than 600 °C can lead to its crystallization and subsequent formation of polycrystalline material.

3. Experiment

Measurements of the absorption spectra and emission spectra were performed with the AVIV 14DS spectrometer (slits: 0.5 mm) and a 0.5 m grating monochromator combined with a photomultiplier tube (PMT) respectively. The decays were detected by a PMT coupled to a SR430 photon counter. As the sources of excitation the Ar-ion, dye and Ti-sapphire lasers and the N_2 laser-pumped dye laser (for decays) were used. A Perkin–Elmer LS50B luminescence spectrometer registered the luminescence excitation spectra. The excited state absorption (ESA) spectra were measured using two alternate setups. One of them was similar to that described in [13] utilizing a CW source of excitation (Ar-ion laser), a tungsten lamp as the source of the probe beam and an optical chopper using a lock-in technique and a 0.4 m grating monochromator plus PMT in the detection branch. The second setup utilized an RD-EXC-150/25 XeCl excimer laser (308 nm) as a source of excitation, a Hamamatsu Xe flash lamp as the source of the probe beam and an ORIEL InstaSpec II photodiode array detector coupled to a MultiSpec 1/8 m spectrograph in the detection branch. The first ESA setup worked in the CW regime and longitudinal geometry of beams passing through the sample, whereas the latter operated in the pulsed regime and transverse geometry (as in [14]).

Describing the results of the basic spectroscopic characteristics, one should first of all note that the obtained optical spectra and fluorescence decays confirmed the results of Henderson *et al* [7–9] and van Die *et al* [15].

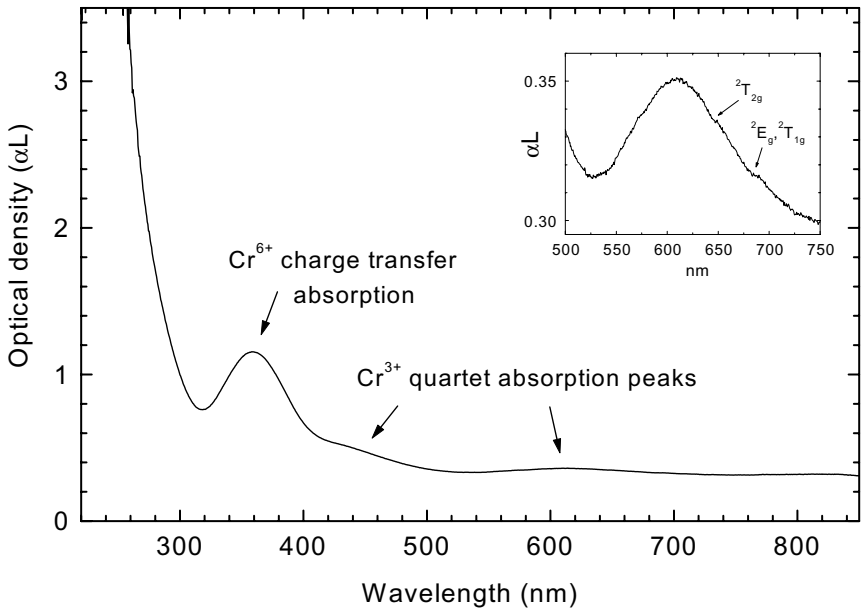

Figure 1. Ground state absorption spectrum of the LBO-glass doped with chromium. Inset shows the magnified $^4T_{2g}$ band affected by doublet features.

Absorption spectrum (figure 1) reveals very distinct features typical for the Cr^{3+} ions (peaks around 420 and 580 nm) and an additional, highest peak, centred at ∼360 nm, which can be ascribed to Cr^{6+} ions [16, 17] (a charge transfer absorption). This absorption, in the frame of the $[CrO_4]^{2-}$ group, is of the following type: $Cr^{6+}O^{2-}(3d^02p^6) \rightarrow Cr^{5+}O^{-}(3d^12p^5)$ [16, 20].

Magnifying the $^4T_2$ band (inset in figure 1) one can see also two distinct features that can be ascribed to $^2T_{2g}$ and ^2E_g, and $^2T_{1g}$ states. Sometimes, in glasses, there are also features connected with Cr^{4+} ions [18, 19]; however this is not evidenced in the observed spectra.

Luminescence excitation spectra (figure 2) were monitored at 688 nm (corresponding to ^2E emission) and 750 nm (corresponding to $^4T_{2g}$ emission). One can note that there is no contribution from Cr^{6+} ion absorption in the observed luminescence of Cr^{3+}. As expected, one can see a typical spectrum with $^4T_{2g}$, $^4T_{1g}$(a) and $^4T_{1g}$(b) peaks. The peak position of the $^4T_{2g}$ band is situated slightly above the R-line region (unlike in typical low-field materials where the R-line falls within the central part of the $^4T_{2g}$ band producing the dip features usually described as Fano antiresonance). The most striking feature of the excitation spectra is the blue shift of the $^4T_{2g}$ peak when monitoring at 688 nm compared to that when monitoring at 750 nm. This appears to be connected with the large degree of site-to-site disorder and, consequently, a wide distribution of the $^4T_{2g}$ states over the energy. A simple mechanism of this blue shift is illustrated in the schematic diagram presented in figure 3. One noted that since the energy of the ^2E_g state depends weakly on the crystal field its absorption and emission is characterized by a sharp line (only slightly broadened) whereas the disordered nature of the glass host is more markedly reflected by the broadening of the $^4T_{2g}$ band. In part (b) of this figure the distribution of the $^4T_{2g}$ state energy is schematically presented. Figure 3(a) shows that exciting the sites of higher crystal field (i.e. higher lying $^4T_{2g}$ states) one actually populates the ^2E_g state whereas when exciting lower lying $^4T_{2g}$ states (low field sites) the metastable state is $^4T_{2g}$ state. This is a reason why the $^4T_{2g}$ band observed at 688 nm is shifted

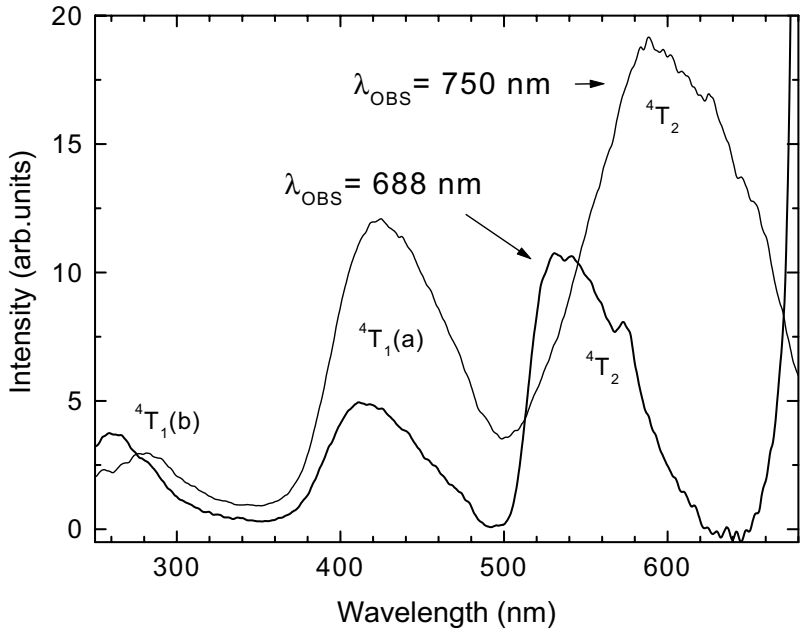

Figure 2. Room-temperature luminescence excitation spectra observed at 688 nm and 750 nm.

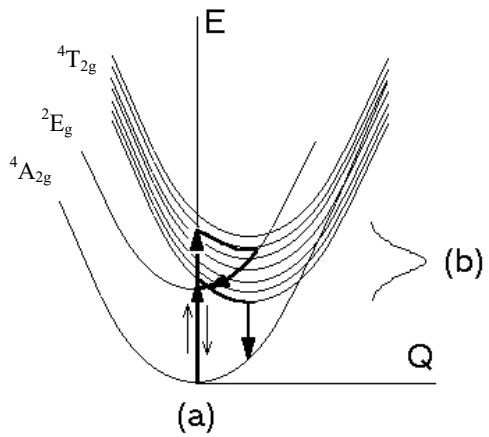

Figure 3. Schematic explanation of the higher energy shift of the $^4T_{2g}$ peak on the excitation spectrum when observing at the R-line (a). Schematic distribution of the $^4T_{2g}$ states over the energy (b).

to shorter wavelengths than the $^4T_{2g}$ band observed at 750 nm. The same cause induces a spectral narrowing of the $^4T_{2g}$(688 nm) band. In such a way the excitation spectrum when monitoring the R-line and the broadband emission allows the identification of the high and low field site absorption. A similar phenomenon, but not that distinct, has been observed by van Die *et al* [15].

Emission spectra were obtained using two types of detector: a PMT and a cooled germanium detector (for wavelengths greater than 800 nm). An exemplary result registered at low (LT) and room (RT) temperature by the germanium detector for excitation at 606 nm

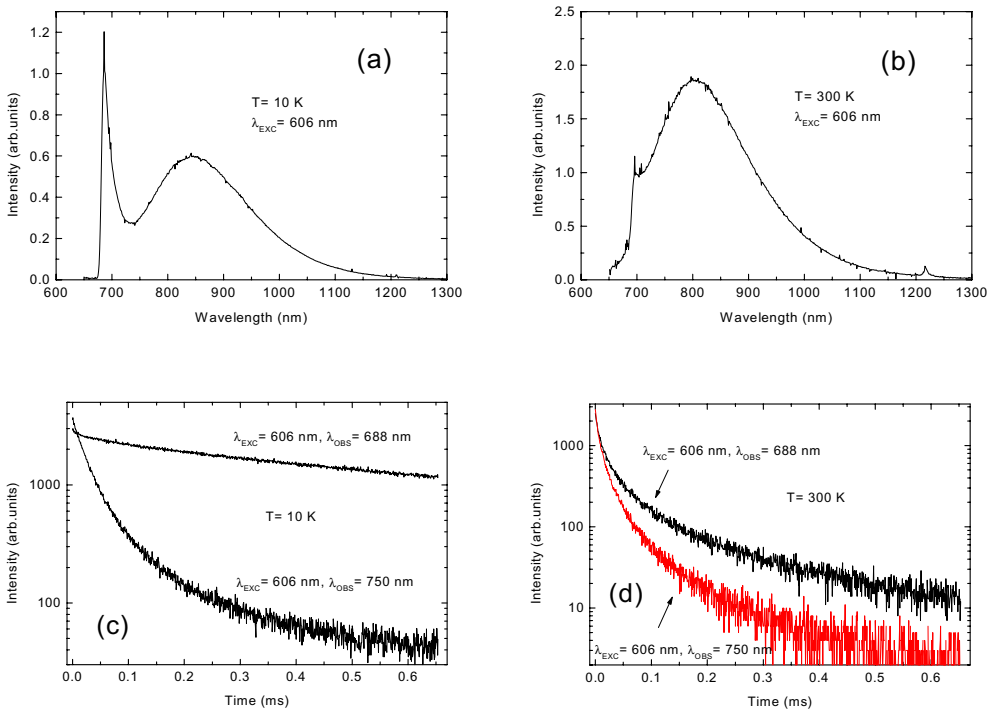

Figure 4. Examples of the luminescence spectra and decays under excitation into the maximum of the $^4T_{2g}$ band detected at low and room temperature.

is illustrated in figures 4(a) and (b). The spectra consist of a distinct peak around ∼688 nm associated with the $^2E_g \rightarrow {}^4A_{2g}$ transitions and the broadband emission of quartet origin ($^4T_{2g} \rightarrow {}^4A_{2g}$). As expected the evidence of the site-to-site disorder in the emission spectra has been observed i.e. exactly the same behaviour as described in [7] and [8] by Henderson *et al* (including the growing contribution of the R-lines for higher excitation energies). Apart from the same observations as in [7] and [8] of the emission characteristics under various excitations, the emission decays at LT and RT have been registered. Fluorescence measurement results for different excitation wavelengths obtained at room temperature (RT) and at 10 K (LT) are presented in figures 4(c) and (d). They clearly show the disordered nature in the luminescence decays being different at LT for $\lambda_{lum} = 688$ nm and $\lambda_{lum} = 750$ nm and thermalized to almost the same, multi-exponential decays at RT, independent of excitation wavelengths.

The intense UV line (363.8 nm) of the Ar-ion laser was used to excite the Cr^{6+} ions into the absorption peak (at 360 nm) ascribed to the charge transfer (CT) absorption. However, only emission from the Cr^{3+} ions was observed, as shown in figure 5. This is partly due to the broad $^4T_{1g}$(a) absorption band of the Cr^{3+} ions extending to the excitation wavelength, partly due to the tail of the $^4T_{1g}$(b) band and perhaps due to the reabsorption of the expected $Cr^{5+}O^-$ emission (the $Cr^{5+}O^-$ centre forms after the CT absorption on the Cr^{6+} ions) in the region of 600–700 nm [20] by the strong $^4T_{2g}$ absorption band (see figure 2). There can also be nonradiative paths of the $Cr^{5+}O^-$ deexcitation in the medium. This nonresult cannot disprove the presence of excited Cr^{6+} ions. Indeed, evidence of excitation of the Cr^{6+} centres and existence of the $Cr^{5+}O^-$ centres (excited form of Cr^{6+}) is observed in excited state absorption (ESA) measurements, discussed in the next section.

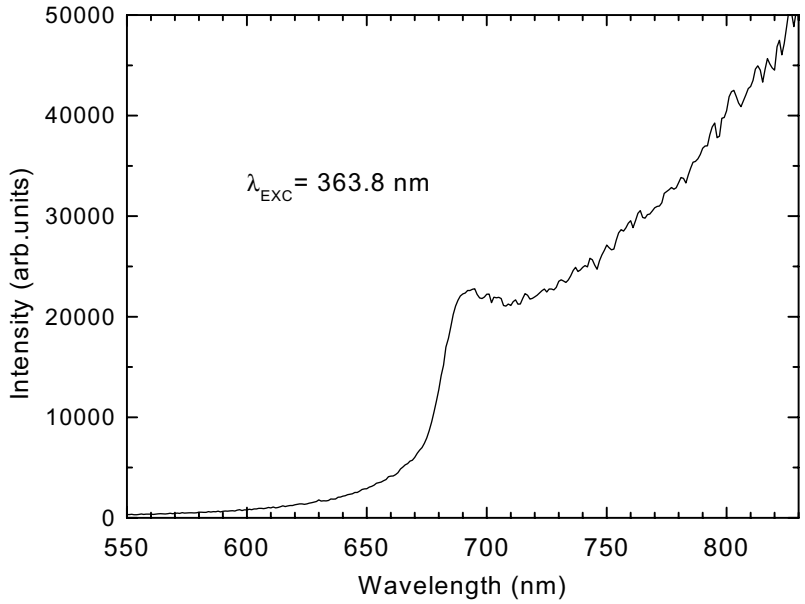

Figure 5. Emission spectrum of the Cr:LBO-glass under excitation into the charge transfer absorption peak of the Cr^{6+} ions.

4. Excited state absorption measurements

The ESA spectra presented in figure 6 have been measured with a number of different excitation wavelengths at room temperature: by Ar laser (488 nm and 514.5 nm), excimer-pumped dye laser (610 nm) and excimer laser (308 nm). The pump wavelength at 308 nm excites the Cr^{6+} ions within the absorption band at 360 nm whereas lines at 488 nm and 610 nm preferentially excite the Cr^{3+} ions. Thus the respective ESA spectra can be considered as resulting from transitions from the metastable states of Cr^{6+} and Cr^{3+}. The excitation wavelength at 514.5 nm has been chosen as an interesting point because it is approximately the intersection of the two quartet peaks of the Cr^{3+} absorption spectrum. The results presented in figure 6 are expressed in terms of the excited state transmission (EST) defined in the following way:

$$\mathrm{EST}(\lambda) = I_p(\lambda)/I_u(\lambda) \tag{1}$$

where I_p is the intensity of the probe beam after passing through the pumped sample and I_u is the same after passing through the unpumped sample.

The most pronounced feature of these spectra is their breadth. For 308 nm and 488 nm excitation an additional peak occurs at ∼400 nm, becomes more pronounced under 514.5 nm excitation and disappears when excitation is at 610 nm.

4.1. Excited state absorption due to Cr^{6+} ions

The ground state absorption (GSA) bleaching can sometimes severely alter the measured EST spectra [21, 22] and it should be eliminated to obtain the true ESA spectra. To do this in a very precise and proper way a knowledge of the concentration N_0 of the optically active centres (Cr) in the ground state and N^* centres in the first excited state is required. Taking also into account the geometry of the measurement and sample size, the obtained ESA spectrum can be

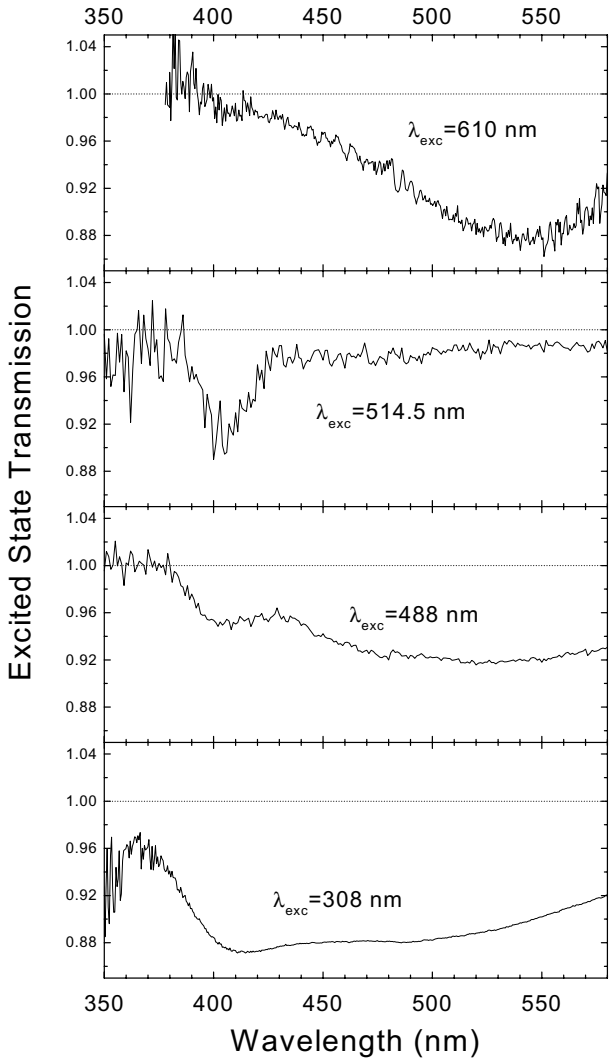

Figure 6. Composition of the EST spectra registered for various excitation wavelengths.

expressed in terms of cross section. However, the LBO-glass, being a very complex structure, does not allow us unambiguously to determine how many chromium ions of a given valence state (Cr^{3+} or Cr^{6+}) reside in distinctly defined sites that could be treated as a reservoir of the ground state ions. To circumvent this problem the ESA spectrum can be re-expressed in terms of the absorption coefficient according to the following formula (e.g. [22]):

$$\alpha_{ESA}(\nu) = \alpha_{ST}(\nu) + \alpha_{GSA}(\nu)\frac{N^*}{N_0} - \frac{\ln[\mathrm{EST}(\nu)]}{L} \tag{2}$$

where α_{ST} is the stimulated emission coefficient and α_{GSA} is the ground state absorption coefficient derived from optical absorption measurement (figure 1). The excitation ratio N^*/N_0 can be treated here as a parameter. $\alpha_{ST}(\nu)$ can be calculated from the emission spectrum $L(\nu)$

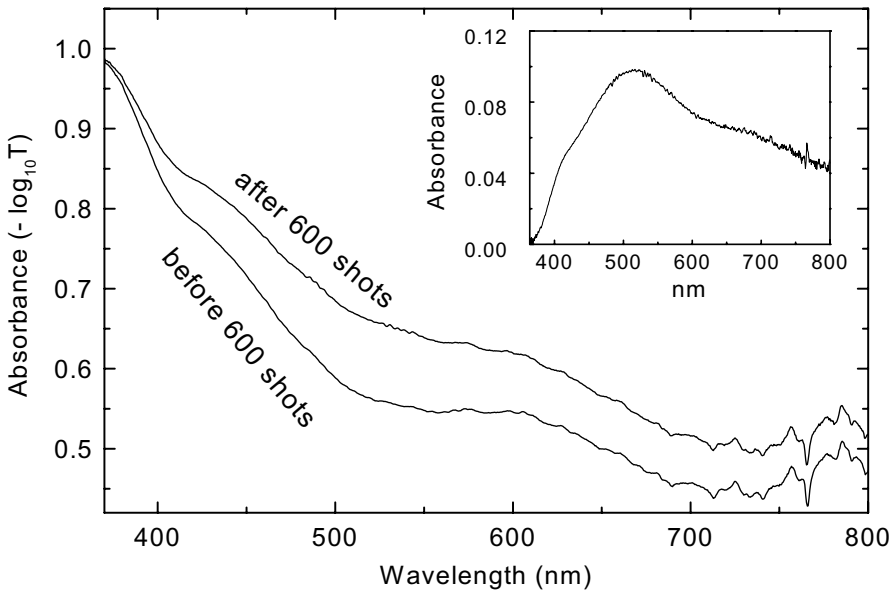

Figure 7. Example of the GSA increase which can cause the GSA bleaching in the measured ESA spectra. The inset shows the absorption spectrum of the induced colour centre.

using the McCumber theory [23, 24]:

$$\alpha_{ST}(\nu) = L(\nu)\left(8\pi\tau_r \int_0^\infty L(\nu)\,\mathrm{d}\nu\right)^{-1}\left(\frac{c}{n\nu}\right)^2 N^* \tag{3}$$

where τ_r is the radiative lifetime of the active ion, n is the refractive index and ν and c are the frequency and velocity of light respectively. Even for an unphysically large population in the first excited state (e.g. $N^* = 5 \times 10^{18}$ cm^{-3}) α_{ST} does not exceed 0.2 cm^{-1}; for most accessible excitation strengths it should be much smaller. The ground state bleaching term $\alpha_{GSA}(\nu)N^*/N_0$ is typically of the order of 0.1 cm^{-1} even for relatively large excitation parameter $N^*/N_0 = 0.01$, and does not exceed 0.25 cm^{-1} in the UV region of interest. Hence the assumption that for practical excitation strength the bleaching as well as stimulated emission should not essentially alter the measured ESA spectrum and thus $\alpha_{ESA}(\nu) \approx -\ln[\mathrm{ESA}(\nu)]/L$.

Exciting by the 308 nm line the presence of yet another GSA bleaching of dynamic character [25] appears to severely influence the ESA results. Figure 7 shows the ground state absorption before and after exposure to 600 shots of excimer laser pulses at 308 nm. The GSA spectra have been measured along the same optical path of the sample as used in the ESA measurements. The presented spectra clearly show induced absorption by the UV excitation (see inset), similarly to other glasses [25] where a build-up of colour centres is observed. The colour centres in glasses are created relatively easily under the intense UV excitation and this also apparently occurs in the LBO-glass. This additional colour centre absorption causes the GSA bleaching which can severely influence the ESA results. The mechanism of such an influence has been described in detail in [22] and [25]. The formation of colour centres appears to be relatively stable until the sample is heated to several hundred °C over a sufficiently long period. Observation in these reversible experiments shows that maintaining the sample at 500 °C for 20 min causes full recovery.

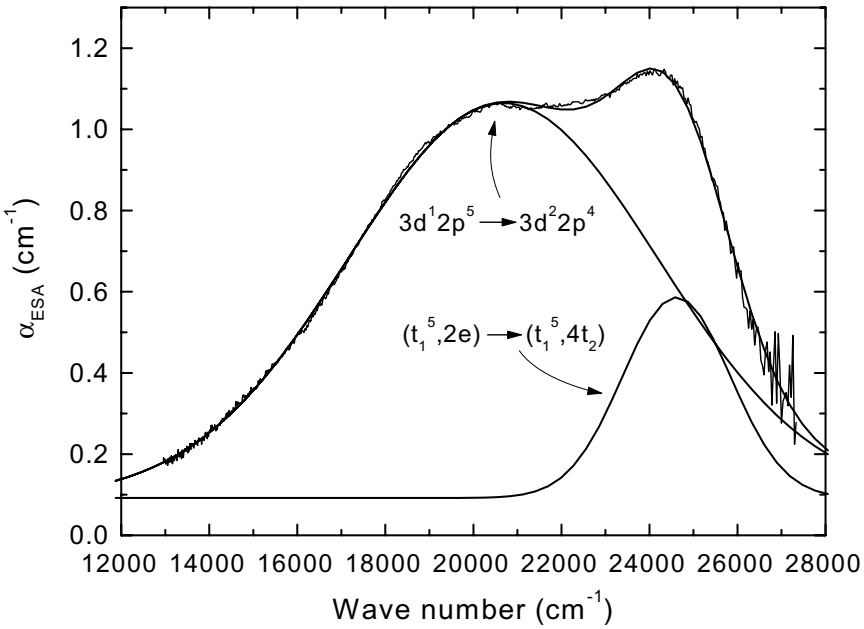

Figure 8. Experimental ESA spectrum obtained for 308 nm excitation, fitted by two Gaussians, and assignation of the contributing ESA bands.

The ESA spectrum of such a recovered sample is presented in figure 8. It shows a little dip between two ESA peaks that might be caused by partial bleaching during this short measurement (100 laser shots). However, as seen, there is no chance to fit this ESA spectrum by a single Gaussian function, whereas two Gaussians (one relatively narrow (2800 cm^{-1}) and another much broader (8200 cm^{-1})) fit the spectrum perfectly. This strongly suggests that the observed ESA under UV excitation consists of transitions to two distinctly defined excited states.

A more precise treatment of the observed data can be attempted constructing a configuration coordinate diagram describing the energetic structure of the Cr^{6+} system. Recently several papers concerning d^0 complexes, treated by very detailed quantum mechanical calculations, have been published (see e.g. [26] and [27]). These papers describe the system in terms of anharmonic vibrations or coupling to the local Jahn–Teller modes.

The spectra obtained in the present work, however, are broad and rather structureless, hence in view of a large variety of the alleged couplings it is pragmatic to model all the couplings by the coupling to an effective mode which represents all active vibrations. Such an effective mode can be described by one collective configuration coordinate. Moreover, one can assume the harmonic approximation and linear electron–lattice coupling. Such an approach allows us at least to avoid a multiparameter fitting in the nine-dimensional space [28], which could be rather a tough task with a lack of detailed experimental data on lower symmetry modes. Hence, it is reasonable to resort to a single configuration coordinate (SCC) model to test and see how far it can lead.

The SCC diagram for the $[CrO_4]^{2-}$ complex obtained with the aforementioned assumptions is illustrated in figure 9. The diagram is based exclusively on the present experimental data, namely ground state absorption (GSA) and ESA spectra. In order to establish the SCC diagram it is necessary to have knowledge of the positions of the maxima

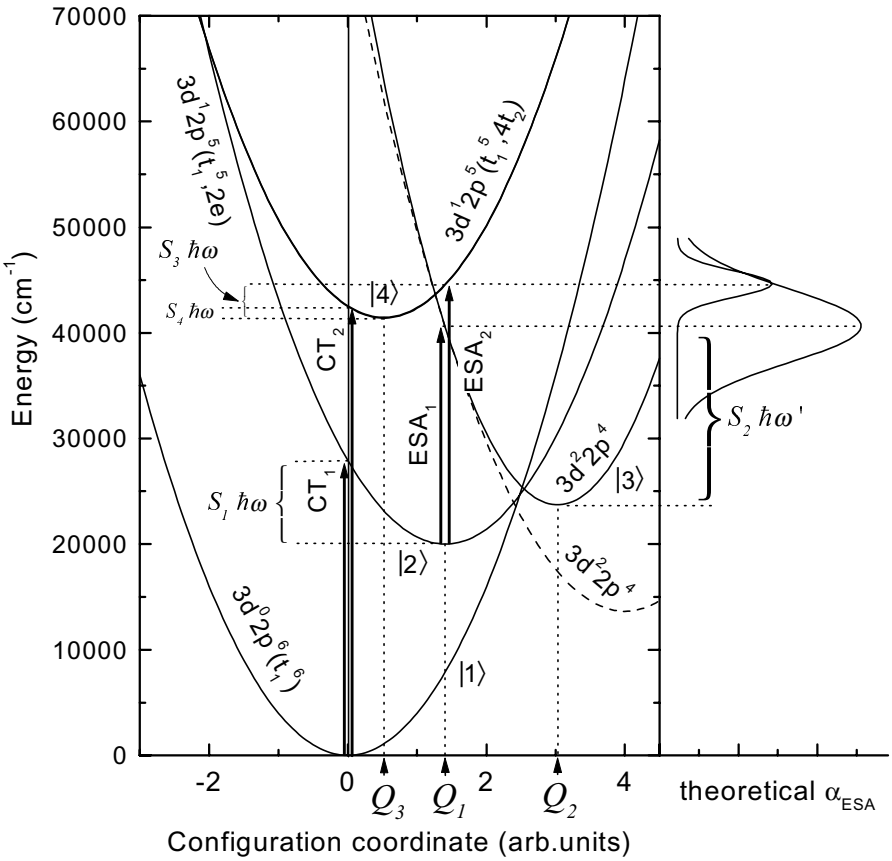

Figure 9. SCC diagram quantitatively reproducing the ESA spectrum obtained with 308 nm excitation. The right side of the figure shows two Gaussian ESA spectra (of the widths corresponding to the respective relaxation energies) whose composition fits the experiment. The dashed parabola corresponds to the $3d^2 2p^4$ state of linear coupling to the lattice, i.e. with the same phonon energy as all remaining states ($\hbar\omega = 250$ cm^{-1}). The solid parabola of the $3d^2 2p^4$ state corresponds to the different phonon energy $\hbar\omega' = 400$ cm^{-1}.

of the GSA and ESA bands and the electron–lattice relaxation energies, $S_i\hbar\omega$, in respective electronic manifolds. The terms defined in figure 9 are related to experimental data as follows: $S_i\hbar\omega, i = 1, \ldots, 4$, relaxation energies corresponding to the respective excited states, CT_1, the energy of the first charge transfer absorption peak, and $ESA_{1,2}$, energies of the ESA maxima. The second charge transfer peak of the energy CT_2 is not seen in the absorption spectrum (CT absorption of the Cr^{6+} ions has always two peaks [16]; here the higher energy peak is assumed to be immersed in the absorption edge of the glass lattice) and therefore is treated as a fitting parameter.

The SCC diagram can be used to reproduce a characteristic ESA spectrum comparable to that obtained with 308 nm excitation (figure 8). To achieve this, a certain assumption has to be made, namely the existence of an additional excited electronic manifold, strongly coupled to the lattice, not detectable in the GSA spectrum. Such a state can be related to the $3d^2 2p^4$ electronic configuration of the central ion–ligand system. A set of energy equations (where energies E_i correspond to states $|i\rangle, i = 1, \ldots, 4$) is obtained assuming a single configuration

coordinate, harmonic oscillations and linear coupling to the lattice of all the states except the state $|3\rangle$ of the energy $E_3(Q)$ (this is discussed below):

$$E_1(Q) = \frac{\kappa}{2}Q^2$$
$$E_2(Q) = \mathrm{CT}_1 - S_1\hbar\omega + \frac{\kappa}{2}(Q - Q_1)^2$$
$$E_3(Q) = \mathrm{CT}_1 - S_1\hbar\omega + \mathrm{ESA}_1 - S_2\hbar\omega' + \frac{\kappa_1}{2}(Q - Q_2)^2 \tag{4}$$

and the highest state E_4 can be expressed in two ways:

$$E_{41}(Q) = \mathrm{CT}_1 - S_1\hbar\omega + \mathrm{ESA}_2 - S_3\hbar\omega + \frac{\kappa}{2}(Q - Q_3)^2$$

or

$$E_{42}(Q) = \mathrm{CT}_2 - S_4\hbar\omega + \frac{\kappa}{2}(Q - Q_3)^2$$

where parameters κ and κ_1 are elastic constants that describe the parabola's curvatures, $\mathrm{CT}_{1,2}$ are energies of the charge transfer absorption maxima, $S_i\hbar\omega$ $(i = 1, \ldots, 4)$ are the appropriate relaxation energies (S is the Huang–Rhys parameter, $\hbar\omega$ is the phonon value) and $\mathrm{ESA}_{1,2}$ are the energies of the broad- and narrow-band ESA maxima respectively. The elastic constant corresponding to the state $|3\rangle$ is $\kappa_1 = \kappa(\hbar\omega'/\hbar\omega)$, where $\hbar\omega'$ is a phonon value corresponding to the state $|3\rangle$. The energy CT_2 acts as a fitting parameter in such a way that for arbitrarily chosen CT_2 there are two highest states (the first calculated according to $E_{41}(Q)$, the second according to $E_{42}(Q)$) whereas only one specific value of CT_2 will produce a single highest state from two (i.e. $E_{41} = E_{42} = E_4$). Hence, this specific CT_2 energy corresponds to the second charge transfer peak in the Cr^{6+} absorption. The fitting value of CT_2 (42 500 cm^{-1}) corresponds to the higher CT peak positioned at $\lambda \cong 235$ nm.

The relaxation energies $S_i\hbar\omega$ $(i = 1, 3, 4)$ are related to the band-widths at half maximum (FWHM), Γ_i, by the following formulae [29, 30]:

$$S_i\hbar\omega = \frac{\Gamma_i^2}{8\ln 2\hbar\omega\coth(\hbar\omega/2kT)} \tag{5}$$

where k is the Boltzmann constant and T is temperature. The relaxation energy $S_2\hbar\omega'$ of the state $|3\rangle$, which has different phonon energy to the other states and is coupled more strongly to the lattice, can be expressed by a more complex formula. Although one can precisely calculate the lineshape and $S_2\hbar\omega'$ from the overlapping integrals of the vibronic functions, for the purpose of this paper it is sufficient to use an approximated relation of the same shape as (5):

$$S_2\hbar\omega' = \frac{\Gamma_2^2}{8\ln 2\hbar\omega'\coth(\hbar\omega/2kT)}. \tag{6}$$

The respective equilibrium points of the i states are situated at the following Q_i:

$$Q_1 = \sqrt{\frac{2S_1\hbar\omega}{\kappa}} \qquad Q_2 = \sqrt{\frac{2S_2\hbar\omega'}{\kappa_1}} + Q_1 \qquad Q_3 = Q_1 - \sqrt{\frac{2S_3\hbar\omega}{\kappa}} \tag{7}$$

and Q_3 in turn enables the determination of the last unknown relaxation energy: $S_4\hbar\omega = (\kappa/2)Q_3^2$.

The resulting SCC diagram calculated using the parameters given in table 1 is presented in figure 9 together with definitions of energies taken from the experiment. It shows two positions of the state $|3\rangle$ ($3d^2 2p^4$) (dashed and solid) corresponding to two qualitatively different situations as described at the end of this section.

Table 1. Parameters used to create the SCC diagram explaining the ESA spectra shown in figure 8.

	κ	$\hbar\omega$	$\hbar\omega'$	kT	CT_1	CT_2	Γ_1	Γ_2	Γ_3	ESA_1	ESA_2
Energy (cm^{-1})	8000	250	400	200	27 933	42 500	4450	8200	2800	20 520	24 600

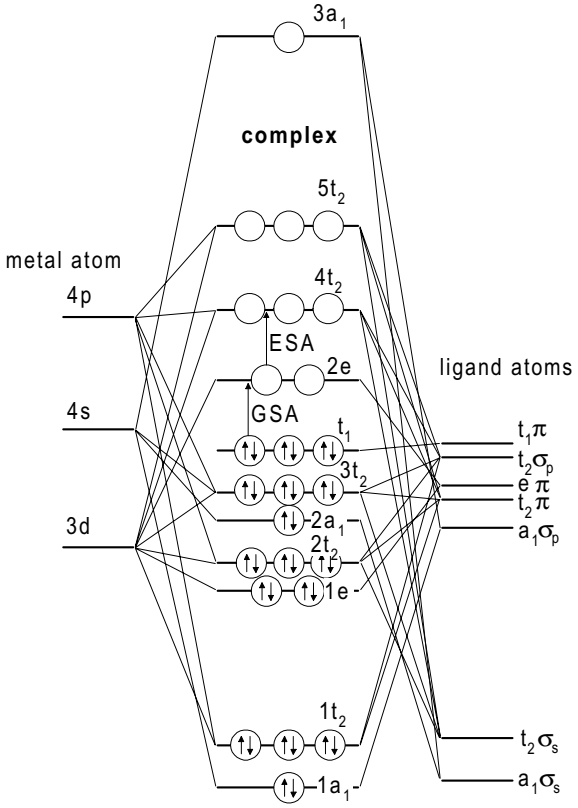

Figure 10. Schematic molecular orbital energy level diagram for MX_4 type complexes (after [31], where the case of the MnO_4^- complex was considered). The GSA and ESA transitions are indicated.

It is worthwhile to note that the described SCC diagram uses only the electronic configurations, not the terms, because complex energetic structure of the Cr^{6+} centre together with its excited states ($Cr^{5+}O^-$) of different spin multiplets (singlets and triplets) would make creation of the SCC diagram impossible without detailed knowledge of the multiplet structure of a given configuration.

Considering the nature of the electronic configurations which the SCC diagram is constructed from, one should remember that the $[CrO_4]^{2-}$ group or, in other words, the $Cr^{6+}O^{2-}$ centre is a typical d^0 complex (of approximate T_d symmetry). Then it is possible to write formally the electronic configuration of the central ion-ligand system as $3d^02p^6$ [20]. The exemplary molecular orbital diagram for the tetrahedral MX_4 complex [31–33] is illustrated in figure 10. It is noted that the highest occupied bonding orbital t_1 of the ground state of such a complex is composed exclusively from ligand p_π orbitals. The higher, nonbonding molecular orbital 2e is of d type and consists mostly of the d orbital of the central ion, whereas the next antibonding orbital $4t_2$ is a typical mixed orbital consisting of the d orbital of the

central ion but also p_σ orbitals of the ligands. This is why the parabola corresponding to $(t_1^5, 4t_2)$ symmetry is shifted with respect to the $(t_1^5, 2e)$ parabola (different charge distributions and consequently different couplings to the lattice). The ground state absorption (CT_1) is due to one of the t_1 electrons, making a transition to the 2e orbital and leaving a hole in the bonds. Because the transition occurs practically from the ligands to the central-ion d orbital, this is what is usually called a 'charge transfer transition', resulting in a distinct charge redistribution. This is consistent with the right-hand shift of the first excited state parabola. There is also another absorption, CT_2, which is involved with a transition of one of the t_1 electrons to the $4t_2$ orbital with suitably smaller charge redistribution. Thus the CT transition transforms the centre $Cr^{6+}O^{2-}$ to the $Cr^{5+}O^-$ centre of $3d^12p^5$ configuration [20]. The larger energy ESA transition (ESA_2) is from the d-type 2e to the more diffused $4t_2$ orbital of mixed d–p type. This is also charge redistribution (simplifying: from the central ion back to the ligands) which results in the $(t_1^5, 4t_2)$ parabola shifted back in respect to the shift of the $(t_1^5, 2e)$ parabola, almost to the same position as the ground state parabola. The smaller energy ESA transition (ESA_1) occurs also from the state of $(t_1^5, 2e)$ configuration but to a state of quite different electronic configuration, namely $3d^22p^4$.

It seems that the most important conclusion obtained from this SCC diagram is the necessity to invoke the existence of one more electronic manifold which is coupled more strongly to the lattice that those of $3d^12p^5$ configuration. The model discussed above and the goodness of the fit to experimental data suggested the manifold involved to be of the $3d^22p^4$ electronic configuration. Such an excited electronic configuration originates from the consecutive excitation of two electrons from the valence band (made up mostly of ligand orbitals) to the d orbitals of the central ion. Actually one can consider this excitation as a double exciton. The very large electron–lattice coupling results from the fact that the redistribution of two electrons has to result in the twofold greater lattice displacement and fourfold greater lattice relaxation energy than in case of single electron redistribution. This effect has been described for the so-called negative U centres [34] and its conditions are quite well satisfied in the present SCC model (figure 9).

Finally the question of which excited electronic manifold, $3d^12p^5(t_1^5, 2e)$ or $3d^22p^4$, is actually the metastable state is discussed. Although the $3d^22p^4$ electronic configuration cannot be reached by the GSA transitions, according to the diagram presented in figure 9 (the version with the dashed $3d^22p^4$ parabola) the system can relax from the $3d^12p^5(t_1^5, 2e)$ electronic manifold to the $3d^22p^4$ electronic configuration, since the latter has lower energy. There are two possible reasons why such a relaxation could not take place. The first can be related to the relatively high energy barrier between $3d^12p^5(t_1^5, 2e)$ and $3d^22p^4$. This barrier though it cannot prevent relaxation can make such a process ineffective and slow. The second possibility corresponds to the solid $3d^22p^4$ parabola in figure 9, i.e. when the minimum energy of the $3d^22p^4$ electronic manifold is higher than that of $3d^12p^5(t_1^5, 2e)$. Such a condition can be satisfied under the assumption that the phonon energies of the respective states will increase according to the relation

$$\hbar\omega_{3d^02p^6} \leqslant \hbar\omega_{3d^12p^5} \leqslant \hbar\omega_{3d^22p^4}. \tag{8}$$

In other words, the second inequality of the relation (8) can be commented on as follows: the state $|3\rangle$ of $3d^22p^4$ configuration is least diffused (most localized) when having two electrons on the central ion (or in more contemporary terms: revealing substantially higher charge in the d orbital of the central ion) and thus binding more strongly the ligand nuclei; then its parabola has larger curvature and the appropriate phonon energies are bigger.

Actually the relation (6) for relaxation energy in the state $|3\rangle$ ($3d^22p^4$) describes the situation when the minimum of $3d^22p^4$ lies above that of $3d^12p^5(t_1^5, 2e)$. This situation is

satisfied as long as the photon energy $\hbar\omega_{3d^2 2p^4} \equiv \hbar\omega'$ is greater than $\sim$330 cm^{-1}, under the assumption that $\hbar\omega_{3d^0 2p^6} = \hbar\omega_{3d^1 2p^5} = 250$ cm^{-1}. In equation (6) the phonon energy $\hbar\omega$ in the coth argument originates from the initial state of the ESA_1 transition, whereas the different phonon energy $\hbar\omega'$ in the denominator originates from the second moment of the ESA_1 lineshape, i.e. from the terminal state of the ESA_1 transition. The SCC diagram presented in figure 9 has been calculated using a still realistic value of the $\hbar\omega'$ phonon energy, 400 cm^{-1}, which makes the state $|3\rangle$ $3d^2 2p^4$ rather unstable, and then the only metastable state is $|2\rangle$ $3d^1 2p^5(t_1^5, 2e)$.

The effect of such nonlinear electron–lattice coupling often takes place when dealing with the Jahn–Teller effect [35] and can also be related to the lattice-confined centres of strong electron–lattice coupling [36, 37]. The quantum confinement makes the second option (expressed by relation (8)) more realistic because the state confinement [36, 37] should be larger with growing number of electrons.

4.2. Excited state absorption due to Cr^{3+} ions

To investigate the ESA associated with the excitation of Cr^{3+} ions the following excitation wavelengths were used: 488, 514.5 and 610 nm. Going back to figure 6, it illustrates the ESA spectra (by means of the EST) obtained for these excitations, comparing them to the EST spectrum for 308 nm excitation. The broadband EST spectrum obtained with 488 nm excitation can be ascribed to the Cr^{3+} ions as this excitation wavelength excites directly the Cr^{3+} ions into the $^4T_{1g}$(a) state. First inspection of the large spectral width might suggest that it is connected with the site-to-site disordered nature of the glass host producing the wide distribution of the initial ESA states, as long as the excitation relaxes to the $^4T_{2g}$ states. Another possibility is connected with a large number of higher energy doublet states acting as the terminating states for the ESA could also produce similar broad ESA band. There is also a third, simplest possibility that the ESA transitions occur from the states of the Cr^{3+} ions to the conduction band of the host.

The first two hypotheses were examined theoretically using a multi-site model based on the method described in [22]. The calculation failed to reproduce the band shapes and positions of the doublet–doublet or quartet–quartet ESA spectra characteristic for Cr^{3+} ions [22, 25, 38]. Hence one can only resort to the third hypothesis, i.e. to the assumption that the broadband ESA spectrum is produced by the transitions from ^2E_g or $^4T_{2g}$ states to the conduction band of the host. A weakly defined shape of these spectra seems to confirm such an assumption. Indeed, the most probable is the possibility of a combination of intra-ion ESA transitions and ion-to-host transitions, the latter being orders of magnitude more intense (much larger absorption cross-section because of relaxed spin and symmetry selection rules) and thus covering the intra-ion ESA spectra effectively and spreading over several thousands of cm^{-1}. The assumption of Cr^{3+} ion to host transition is confirmed by the ESA observation when the pump wavelength is at 514.5 nm (i.e. between $^4T_2$ and $^4T_1$(a) states). The resulting EST spectrum reveals only a relatively sharp peak around 400 nm. The position and FWHM of this peak does not allow us to ascribe this feature either to charge-transfer-induced ESA in the frame of the $[CrO_4]^{2-}$ complex or to doublet–doublet ESA in the frame of Cr^{3+}. Although a clear interpretation of this peak is still absent at present it reveals the possibility of excitation of some specific yet unknown centre but probably not in the trivalent state of the chromium ions. The EST spectrum under pump excitation at 610 nm (see figure 6) reveals a broad band, confirming the earlier assumption that the ESA transitions are from the Cr^{3+} states to the host conduction band.

5. Conclusions

Two types of ESA characteristic have been observed in the LBO-glass system doped with chromium ions. One of them, occurring under UV (308 nm) excitation, is connected with transitions within the $Cr^{5+}O^{-}$ centre which forms after absorption of charge transfer type in the tetrahedrally coordinated $[CrO_4]^{2-}$ complex. Such a complex, being a typical d^0 system reveals two excited $3d^12p^5$ configurations of the following symmetries: $(t_1^5, 2e)$ and $(t_1^5, 4t_2)$, distanced by 10 Dq energy (in terms of the crystal field approximation), the first being the initial state for the ESA transition, the second being the terminal ESA state. This explains a narrower ESA band. The second, much broader ESA band can only be explained with the assumption of invoking the addition of one more excited configuration ($3d^22p^4$) which forms after transition of the next electron from ligands orbitals to the d orbital of the central ion. Such a configuration, having a very different charge distribution to $3d^12p^5$, is more strongly coupled to the lattice. The ESA transition from $(t_1^5, 2e)$ to the strongly lattice-coupled $3d^22p^4$ state results in the broad ESA band, as illustrated in figure 9.

The existence of the $3d^22p^4$ state may play a role in the lack of effective emission under UV excitation. Either $(t_1^5, 2e)$ or $3d^22p^4$ are strongly coupled to the lattice, having a cross-over point approximately in the same position as between $(t_1^5, 2e)$ and the ground state (t_1^6). Hence non-radiative deexcitation process can occur from both states.

The second type of ESA observed under 488 and 610 nm excitation is connected with transitions from the states of octahedrally coordinated Cr^{3+} ions to the states of the host conduction band. The only ESA feature that does not find interpretation is a relatively sharp ESA peak under 514.5 nm excitation. It can be connected with some unintentional centre e.g. some sort of colour centre that can be most effectively excited by the 514.5 nm line.

Considering the GSA spectra one can see that in glasses the absorption bands related to $^4A_{2g} \rightarrow {}^4T_{2g}$ and $^4A_{2g} \rightarrow {}^4T_{1g}(a)$ transitions in the Cr^{3+} ion are immersed in the much broader absorption whose coefficient increases with excitation energy. This broadband absorption is usually attributed to the band-to-band transitions in the glass host. The ESA spectra presented here show the possibility of transitions from the $^4T_{2g}$ or ^2E_g states of the Cr^{3+} ions to the band states of the host. In the authors' opinion the glasses possess a quite rich density of states, energetically placed in the band gap, which are related to the disorder nature of the glasses. Although these states are probably spatially localized there is substantial overlapping between them and the $3d^3$ electrons of the Cr^{3+} centres. Therefore the transition between d states and these disorder-induced states can be more probable than d–d transitions in the Cr^{3+} ions. In fact, the d–d transitions are parity forbidden, whereas the transitions from the Cr^{3+} ion to the disorder-induced states (most likely to be d–dp or d–p type transitions) are determined mostly by spatial overlapping of the respective wavefunctions.

This conclusion is very negative as far as the possibility of laser operation in chromium-doped LBO-glasses is concerned. The lack of the d–d features in the Cr^{3+} ESA spectra means that the transitions from $^4T_{2g}$ or ^2E_g states to the disorder-induced states are in fact much more probable than d–d transitions. This results in the broad ESA band, overlapping the spectral range of the Cr^{3+} emission and thus killing the possibility of laser action.

Acknowledgments

This work was supported by the State Committee for Scientific Research (KBN) under grant numbers 2 P03B 117 16 and 2 P03B 063 16 and by the Rector of the Nicholas Copernicus University in Toruń, who made possible the visit to the University of Strathclyde, Glasgow, for the collaborative work.

References

[1] Komatsu R, Sugawara T, Sassa K, Sakura N, Liu Z, Izumida S, Segawa Y, Uda S, Fukuda T and Yamanouchi K 1997 *Appl. Phys. Lett.* **70** 3492
[2] Ciocan A, Uebbing J and Niemax K 1992 *Spectrochim. Acta* B **47** 611
[3] Gasiot J, Braunlich P and Fillard J P 1982 *J. Appl. Phys.* **53** 5200
[4] Maiman T H 1960 *Phys. Rev. Lett.* **4** 564
[5] Payne S A, Chase L L, Smith L K, Kway W L and Newkirk H W 1989 *J. Appl. Phys.* **66** 1051
[6] Seo J T, Hömmerich U, Trivedi S B, Chen R J and Kutcher S 1998 *Opt. Commun.* **153** 267
[7] Rasheed F, O'Donnell K P, Henderson B and Hollis D B 1991 *J. Phys.: Condens. Matter* **3** 3825
[8] Henderson B, Yamaga M, Gao Y and O'Donnell K P 1992 *Phys. Rev.* B **46** 652
[9] Yamaga M, Gao Y, O'Donnell K P and Henderson B 1992 *J. Lumin.* **53** 457
[10] Majchrowski A 1995 *Proc. SPIE* **2373** 98
[11] Liebertz J 1983 *Prog. Cryst. Growth Character.* **6** 361
[12] Lukasiewicz T and Majchrowski A 1991 *Mater. Lett.* **11** 281
[13] Wegner T and Petermann K 1989 *Appl. Phys.* B **49** 275
[14] Koepke Cz, Wojtowicz A J and Lempicki A 1993 *J. Lumin.* **54** 345
[15] van Die A, Blasse G and van der Weg W F 1985 *J. Phys. C: Solid State Phys.* **18** 3379
[16] Murata T, Torisaka M, Takebe H and Morinaga K 1997 *J. Non-Cryst. Solids* **220** 139
[17] Casalboni M, Ciafardone V, Giuli G, Izzi B, Paris E and Proposito P 1996 *J. Phys.: Condens. Matter* **8** 9059
[18] Hömmerich U, Eilers H, Yen W M, Hayden J S and Aston M K 1994 *J. Lumin.* **60/61** 119
[19] Stręk W, Łukowiak E, Dereń P J, Maruszewski K, Trabjerg I, Koepke Cz, Malashkevich G E and Gaishun V I 1997 *Proc. SPIE* **3176** 249
[20] Yuan H, Jia W, Cohen D, Yen W M and Aitken B G 1997 *Mater. Res. Soc. Symp. Proc.* **455** 483
[21] Payne S A, Chase L L and Wilke G D 1988 *Phys. Rev.* B **37** 998
[22] Koepke Cz, Wiśniewski K, Grinberg M. Russell D L, Holliday K and Beall G H 1998 *J. Lumin.* **78** 135
[23] McCumber D E 1964 *Phys. Rev.* A **134** 299
[24] Wojtowicz A J, Meng W, Lempicki A, Beall G H, Hall D W and Chin T C 1988 *IEEE J. Quantum Electron.* **24** 1109
[25] Koepke Cz, Wiśniewski K, Grinberg M, Russell D L and Holliday K 1999 *J. Lumin.* **81** 301
[26] Stückl A C, Daul C A and Güdel H U 1997 *J. Chem. Phys.* **107** 4606
[27] Wissing K, Barriuso M T, Aramburu J A and Moreno M 1999 *J. Chem. Phys.* **111** 10 217
[28] Sturge M D 1967 The Jahn–Teller effect in solids *Solid State Physics, Advances in Research and Applications* ed F Seitz, D Turnbull and H Ehrenreich (New York: Academic) pp 91–211
[29] Stoneham A M 1975 *Theory of Defects in Solids, Electronic Structure of Defects in Insulators and Semiconductors* (Oxford: Clarendon) pp 310–17
[30] Henderson B and Imbusch G F 1989 *Optical Spectroscopy of Inorganic Solids* (Oxford: Clarendon) pp 206–8, 285–8
[31] Ballhausen C J and Gray H B 1964 *Molecular Orbital Theory* (New York: Benjamin) pp 123–8
[32] Karplus M and Porter R N 1970 *Atoms and Molecules; an Introduction for Students of Physical Chemistry* (New York: Benjamin)
[33] Figgis B N 1966 *Introduction to Ligand Fields* (New York: Interscience–Wiley) pp 196–200
[34] Toyozawa Y 1985 Electron-induced lattice instabilities *Highlights of Condensed-Matter Theory (LXXXIX Corso)* (Bologna: Societa Italiana di Fisica) pp 797–830
[35] Grinberg M and Mandelis A 1994 *Phys. Rev.* B **49** 12 496
[36] Grinberg M, Jaskólski W, Koepke Cz, Planelles J and Janowicz M 1994 *Phys. Rev.* B **50** 6504
[37] Grinberg M and Jaskólski W 1997 *Phys. Rev.* B **55** 5581
[38] Fairbank W M, Klauminzer G K and Schawlow A L 1975 *Phys. Rev.* B **11** 60